encit 2020

ABCM Associação Brasileira de Engenharia e Ciências Mecânicas

18th Brazilian Congress of Thermal Sciences and Engineering
November 16–20, 2020 (Online)

ENC-2020-0519
DIRECT AND INVERSE ANALYSIS OF THE BIOHEAT EQUATION EMPLOYING INTEGRAL TRANSFORMS AND SURROGATE MODELS

Taciano Magela de Souza Monteiro de Barros
Gisele Moraes Marinho
Luiz Alberto da Silva Abreu
Diego Campos Knupp
Instituto Politécnico, Universidade do Estado do Rio de Janeiro, Nova Friburgo, RJ, Brazil
taciano@iprj.uerj.br, giselemarinho11@gmail.com, luiz.abreu@iprj.uerj.br, diegoknupp@iprj.uerj.br

Abstract. *This paper addresses the heat transfer process within living tissues, as modeled by Pennes' equation, with spatially variable parameters across the tissue thickness to account for different tissues: epidermis, dermis, subcutaneous and inner tissue. The solution of this problem may be of major relevance in applications such as clinical diagnostics employing infrared thermography, burn injuries evaluation and hyperthermia cancer treatments, but it requires the accurate knowledge of the thermophysical properties and blood perfusion rates, which are generally obtained with the solution of the corresponding inverse heat conduction problems. Hence, the main goal of this research is performing the direct and inverse analysis of this bioheat model by combining the Generalized Integral Transform Technique with single domain formulation and Bayesian inference. In the direct problem solution, to allow faster convergence of the eigenfunction expansions, the eigenvalue problem is formulated including as much information as possible, with all the spatially variable properties included. In the inverse problem analysis, to allow for faster sampling of the sought posterior probability densities, a surrogate model based on Radial Basis Functions is employed for the prediction of temperature distributions. The results obtained demonstrate that the use of the metamodel in the inverse problem can significantly reduce computational time, besides the good estimates obtained with the employed approach.*

Keywords: *Bioheat transfer, Integral Transform, Metamodel, Bayesian Inference*

1. INTRODUCTION

The precise prediction of temperature distributions in living tissues has been a research topic in thermal sciences with applications in cryopreservation, cryosurgery, cancer treatment using diathermy, hyperthermia and thermal ablation (Diller et al., 2000). Microwave ablation, for example, is a type of treatment for cancer hyperthermia that involves heating tumor cells. This technique uses electromagnetic wave effects to kill cancer cells (Selmi et al., 2019; Kabiri and Talaee, 2019).

The investigation of heat transfer and fluid flow in biological processes requires reliable mathematical models. The physical-mathematical model commonly used in bio-heat transfer in biological tissues is based on Pennes' equation (Pennes, 1948). This equation incorporates terms that represent the effects of metabolism, blood perfusion and external heat sources (Jiang et al., 2002).

Several analytical solutions provided in the literature represent the distribution of temperature across tissue structures, but are restricted to situations with uniform thermophysical properties over the entire length of the tissue. Cotta et al. (2010) advanced this study considering a single domain formulation in a heterogeneous medium with spatially variable parameters, with constant thermophysical properties in each layer of the tissue. The Generalized Integral Transform Technique (GITT) is used to produce an analytical-numerical solution of the heat biotransference model and the eigenvalue problem is treated with constant coefficients (Cotta, 1993). The single domain formulation was considered in this study, but the solution was constructed with a series expansion upon simpler eigenfunctions, obtained from an eigenvalue problem with constant coefficients.

Still concerning the single domain formulation concept, Knupp et al. (2012), employed GITT in combined conduction-convection heat transfer problems in heterogeneous media, proposing a single domain formulation to model fluid flow and channel wall regions , demonstrating that the use of an eigenvalue problem with spatially variable coefficients to construct the basis of the eigenfunction expansion can remarkably improve the solution convergence rates.

Even with such analytical based solutions at disposal, the search for lower cost solutions still remains of major relevance, specially when dealing with computationally intensive problems, such as optimization and inverse problems. Studies on the metamodeling techniques have been used in several branches of science, mainly in engineering reliability

analysis to reduce the time to solve such problems. A comparative study on metamodeling techniques was developed by Jin et al. (2001) using different modeling criteria on a variety of test problems. Orlande et al. (2008) used RBF to interpolate the likelihood function applied to inverse heat and mass transfer problems and obtained a significant reduction in computational cost without loss of precision in the results.

The present work addresses a problem of heat transfer in a one-dimensional domain with multi-layered tissue, such the one tackled by Cotta et al. (2010). The domain is treated as a heterogeneous medium using the single domain formulation, so that the heat flow and temperature continuity are satisfied at the interfaces and a single equation is used for the entire domain. The auxiliary eigenvalue problem is formulated by directly applying the separation of variables to the homogeneous version of the original problem, so that all information related to the transition between layers is represented by the coefficients with spatial variation of the eigenvalue problem, which in this case, is resolved with GITT. The Markov chain Monte Carlo method (MCMC) is used in the analysis of the inverse problem that consists in estimate the blood perfusion term. To allow for a faster sampling of the posterior probability densities, a surrogate model based on Radial Base Functions (RBFs) is used to calculate the temperature distributions.

2. PROBLEM FORMULATION

Consider a linear heat conduction problem in a biological system in which the temperature field, $T(x,\, t)$, is modeled by a partial differential equation as given by the Pennes' equation with spatially variable properties and defined by (Cotta et al., 2010) as:

$$w(x)\frac{\partial T(x,\, t)}{\partial t} = \frac{\partial}{\partial x}\left[k(x)\frac{\partial T(x,\, t)}{\partial x}\right] + P(x,\, t,\, T), \qquad 0 < x < L, \qquad t > 0 \tag{1}$$

$$T(x,\, t) = T_p(x), \qquad 0 < x < L, \qquad t = 0 \tag{2}$$

$$-k(x)\frac{\partial T(x,\, t)}{\partial x} = q(t) + h[T_\infty(t) - T(x,\, t)], \qquad x = 0, \qquad t > 0 \tag{3}$$

$$\frac{\partial T(x,\, t)}{\partial x} = 0, \qquad x = L, \qquad t > 0 \tag{4}$$

where,

$$w(x) = \rho(x)c_p(x), \qquad P(x,\, t,\, T) = q_m(x,\, t) + \omega(x,\, T)\rho_b c_b[T_a - T(x,\, t)] \tag{5, 6}$$

where L is the tissue layer thickness, $w(x)$ is the thermal capacity of tissue, $\rho(x)$ is the specific mass of tissue, $c_p(x)$ is the specific heat of tissue, $k(x)$ is the thermal conductivity of tissue, $q(t)$ is the applied wall heat flux, h is the effective heat transfer coefficient, $T_\infty(t)$ is external environment temperature, $\omega(x,\, T)$ is a term related to blood perfusion rates, ρ_b is the specific mass of blood, c_b is the specific heat of blood, $q_m(x,\, t)$ is the metabolic heat generation, T_a is the arterial blood temperature, $T_p(x)$ is the steady-state solution.

Figure 1 presents a schematic diagram of the heterogeneous tissue for a characteristic one-dimensional transient heat transfer problem. Tissues are assumed to be homogeneous within each layer. The initial condition, Eq. (2), is obtained from the steady-state solution for the situation without external stimulus, i.e., $q(t) = 0$, and constant external environment temperature.

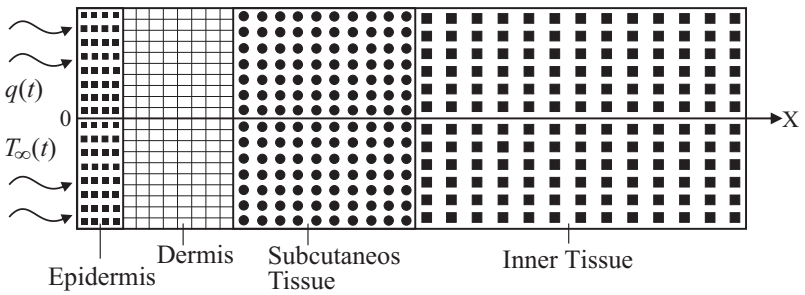

Figure 1. Schematic diagram of the heterogeneous tissue. Adapted from Cotta et al. (2010)

2.1 Formulation of the direct problem

In this work, it is applied the so-called single domain formulation that allows a more straightforward treatment of the chosen model, where coefficients with abrupt spatial variation are introduced into the equation. A filtering solution is employed in order to improve the convergence behavior of the eigenfunction expansions, in the form:

$$T(x,\,t) = T_f(x;\,t) + T^*(x,\,t) \tag{7}$$

The filtering solution is written as a linear function in the space variable that simultaneously satisfies both boundary conditions, Eqs. (3)-(4), and it is given by:

$$T_f(x;\,t) = T_\infty(t) + \frac{q(t)}{h} \tag{8}$$

This solution homogenizes the boundary conditions in the filtered partial differential problem to be integral transformed. The filtered temperature problem formulation is written in the form:

$$w(x)\frac{\partial T^*(x,\,t)}{\partial t} = \frac{\partial}{\partial x}\left[k(x)\frac{\partial T^*(x,\,t)}{\partial x}\right] + P^*(x,\,t,\,T), \qquad 0 < x < L, \qquad t > 0 \tag{9}$$

$$T^*(x,\,t) = f(x) \equiv T_p(x) - T_f(x;\,t), \qquad 0 < x < L, \qquad t = 0 \tag{10}$$

$$-k(x)\frac{\partial T^*(x,\,t)}{\partial x} + hT^*(x,\,t) = 0, \qquad x = 0, \qquad t > 0 \tag{11}$$

$$\frac{\partial T^*(x,\,t)}{\partial x} = 0, \qquad x = L, \qquad t > 0 \tag{12}$$

where the filtered term is written as:

$$P^*(x,\,t,\,T) = -\omega(x,\,T)\rho_b c_b T^*(x,\,t) + q_m(x,\,t) + \omega(x,\,T)\rho_b c_b[T_a - T_f(x;\,t)] - w(x)\frac{\partial T_f(x;\,t)}{\partial t} \tag{13}$$

The formal solution of problem (9)-(13) is then obtained with the Generalized Integral Transform Technique, and is written as the inverse formula below:

$$T^*(x,\,t) = \sum_{i=1}^{NT} \tilde{\Psi}_i(x)\bar{T}_i(t), \qquad \textit{inverse} \tag{14}$$

where NT is a sufficiently large finite truncation order and the transformed potentials are defined with the integral transformation operation given by:

$$\bar{T}_i(t) = \int_0^L w(x)\tilde{\Psi}_i(x)T^*(x,\,t)dx, \qquad \textit{transform} \tag{15}$$

where $\tilde{\Psi}_i(x)$ are the normalized eigenfunctions and N_i are the normalization integrals:

$$\tilde{\Psi}_i(x) = \frac{\Psi_i(x)}{\sqrt{N_i}}, \qquad N_i = \int_0^L w(x)\Psi_i^2(x)dx \tag{16, 17}$$

The eigenvalues μ_i and eigenfunctions $\Psi_i(x)$ are obtained from the eigenvalue problem defined by:

$$\frac{d}{dx}\left[k(x)\frac{d\Psi_i(x)}{dx}\right] + \mu_i^2 w(x)\Psi_i(x) = 0, \qquad x \in [0,\,L] \tag{18}$$

with boundary conditions:

$$-k(0)\left.\frac{d\Psi_i(x)}{dx}\right|_{x=0} + h\Psi_i(0) = 0, \qquad \left.\frac{d\Psi_i(x)}{dx}\right|_{x=L} = 0 \tag{19, 20}$$

The eigenvalue problem (18)-(20) does not allow for closed form solution, and the GITT is used to provide a simpler auxiliary eigenvalue problem. The simplified auxiliary eigenvalue problem is represented as follows:

$$\frac{d}{dx}\left[\hat{k}(x)\frac{d\Omega_n(x)}{dx}\right] + \lambda_n^2\hat{w}(x)\Omega_n(x) = 0, \qquad x \in [0,\,L] \tag{21}$$

and the boundary conditions are defined as:

$$-\hat{k}(0)\frac{d\Omega_n(x)}{dx}\bigg|_{x=0} + \hat{h}\Omega_n(0) = 0, \qquad \frac{d\Omega_n(x)}{dx}\bigg|_{x=L} = 0 \tag{22, 23}$$

and the coefficients $\hat{k}(x)$, $\hat{w}(x)$ and $\hat{h}$ are chosen so as to admit an analytical solution to the auxiliary problem.

The solution of problem (21)-(23) offers a basis itself for the eigenfunction expansion of the original eigenvalue problem, Eqs. (18)-(20). The expansion of the original eigenfunction is then written as:

$$\Psi_i(x) = \sum_{n=1}^{NT^*} \tilde{\Omega}_n(x)\bar{\Psi}_{i,n}, \qquad \textit{inverse} \tag{24}$$

$$\bar{\Psi}_{i,n} = \int_0^L \hat{w}(x)\tilde{\Omega}_n(x)\Psi_i(x)dx, \qquad \textit{transform} \tag{25}$$

where NT^* is the number of terms in the expansion of the original eigenfunction and the auxiliary normalized eigenfunctions, $\tilde{\Omega}_n(x)$, and the auxiliary normalization integrals, N_{Ω_n}, are given by:

$$\tilde{\Omega}_n(x) = \frac{\Omega_n(x)}{\sqrt{N_{\Omega_n}}}, \qquad N_{\Omega_n} = \int_0^L \hat{w}(x)\Omega_n^2(x)dx \tag{26, 27}$$

In the present work, the simplest possible choice is considered, with $\hat{k}(x) = 1$, $\hat{w}(x) = 1$ and $\hat{h} = h/k(x)$. The integral transformation of the eigenvalue problem with space variable coefficients is then performed by operating on Eq. (18) with $\int_0^L \tilde{\Omega}_m(x)(\cdot)dx$, to yield the following algebraic problem in matrix form (Knupp et al., 2012):

$$(\mathbf{A} - \mu^2\mathbf{B})\bar{\mathbf{\Psi}} = 0, \tag{28}$$

where the matrix $\mathbf{A}$ and $\mathbf{B}$ are defined by:

$$\mathbf{A} = \{A_{n,m}\}, \qquad A_{n,m} = -\left[k(x)\tilde{\Omega}_m(x)\frac{d\tilde{\Omega}_n(x)}{dx}\right]_{x=0} - \int_0^L k(x)\frac{d\tilde{\Omega}_n(x)}{dx}\frac{d\tilde{\Omega}_m(x)}{dx}dx \tag{29}$$

$$\bar{\mathbf{\Psi}} = \{\bar{\Psi}_{n,m}\}; \qquad \mathbf{B} = \{B_{n,m}\}, \qquad B_{n,m} = \int_0^L w(x)\tilde{\Omega}_n(x)\tilde{\Omega}_m(x)dx \tag{30}$$

The algebraic problem, Eq. (28), is numerically solved providing results for the eigenvalues, μ^2, and their respective eigenvectors, $\bar{\mathbf{\Psi}}$, which combined with the inverse formula, Eq. (24), provide original eigenfunctions, $\Psi_i(x)$.

The integral transformation is now performed by operating on Eq. (9) with $\int_0^L \tilde{\Psi}_i(x)(\cdot)dx$, providing the following transformed ordinary differential system:

$$\frac{d\bar{T}_i(t)}{dt} + \mu_i^2\bar{T}_i(t) = \bar{g}_i(t, \bar{T}_j), \qquad i, j = 1, 2, ..., NT \tag{31}$$

with the transformed source terms given by:

$$\bar{g}_i(t, \bar{T}_j) = \int_0^L \tilde{\Psi}_i(x)P^*(x, t, T)dx \tag{32}$$

and the transformed initial conditions is obtained after operating Eq. (10) with $\int_0^L w(x)\tilde{\Psi}_i(x)(\cdot)dx$:

$$\bar{T}_i(0) = \int_0^L w(x)f(x)\tilde{\Psi}_i(x)dx, \qquad i = 1, 2, ..., NT \tag{33}$$

The transformed ordinary differential system, Eq. (31), after truncation to a finite order NT, is numerically solved by the NDSolve routine of *Mathematica* and combined by the inverse formula, Eq. (14), to produce the temperature field, $T^*(x, t)$. The original temperature field, $T(x, t)$, is obtained using Eq. (7).

2.2 Radial Basis Function

The Radial Base Function (RBF) is a metamodeling technique based on interpolation. The method operates linear combinations of a radially symmetric function based on Euclidean distance or another metric to approximate the response functions. This technique consists of obtaining a function $\widehat{\mathbf{T}}(\mathbf{x})$ that has the following form (Fornberg et al., 2006):

$$\widehat{\mathbf{T}}(\mathbf{x}) = \sum_{k=1}^{N} p_k \varphi(\| \mathbf{x} - \mathbf{x}_k \|) = \sum_{k=1}^{N} p_k \sqrt{(\mathbf{x} - \mathbf{x}_k)^2 + \eta_k^2} \qquad \forall\ (\mathbf{x} - \mathbf{x}_k) \in \mathbb{R} \text{ e } \eta > 0 \tag{34}$$

where $\widehat{\mathbf{T}}$ is the estimated temperature vector, N is the number of points used in the interpolation, p_k are the weights (unknown coefficients), φ is a set of N multi-quadratic radial base functions, $\| \cdot \|$ denotes the Euclidean norm, $\mathbf{x}$ are the function's input parameters, $\mathbf{x}_k$ denotes the central value of the associated function and η_k symbolizes the value of the RBF width.

The weights are determined by solving a set of N simultaneous linear equations given by (Haykin, 2008):

$$\begin{bmatrix} \varphi_{11} & \varphi_{12} & \cdots & \varphi_{1N} \\ \varphi_{21} & \varphi_{22} & \cdots & \varphi_{2N} \\ \vdots & \vdots & \ddots & \vdots \\ \varphi_{N1} & \varphi_{N2} & \cdots & \varphi_{NN} \end{bmatrix} \begin{bmatrix} p_1 \\ p_2 \\ \vdots \\ p_N \end{bmatrix} = \begin{bmatrix} T_1 \\ T_2 \\ \vdots \\ T_N \end{bmatrix}, \tag{35}$$

where

$$\varphi_{ik} = \varphi(\| \mathbf{x}_i - \mathbf{x}_k \|), \qquad i, k = 1, 2, ..., N \tag{36}$$

$$\mathbf{p} = [p_1, p_2, ..., p_N]^T, \qquad \widehat{\mathbf{T}} = [T_1, T_2, ..., T_N]^T \tag{37, 38}$$

where $\mathbf{p}$ and $\widehat{\mathbf{T}}$ represent the linear weight vector and the desired response vector obtained by GITT, respectively, see Eq. (7). Defining $\mathbf{\Phi}$ as an interpolation matrix with the elements φ_{ik}:

$$\mathbf{\Phi} = \{\varphi_{ik}\}_{i,\, k=\mathbf{1}}^{N} \tag{39}$$

than, Eq. (35) can be rewritten in its compact form:

$$\mathbf{\Phi p} = \widehat{\mathbf{T}} \tag{40}$$

Assuming that the matrix $\mathbf{\Phi}$ is non-singular, than it is assumed that there is an inverse matrix, $\mathbf{\Phi^{-1}}$, the solution of Eq. (40) is then obtained for the weight vector as:

$$\mathbf{p} = \mathbf{\Phi^{-1}} \widehat{\mathbf{T}} \tag{41}$$

3. FORMULATION OF THE INVERSE PROBLEM

In the Bayesian approach, an attempt is made to use the available information to reduce the amount of uncertainty present in a given inferential problem. As new information is obtained, it is added with the existing information to form the basis for statistical procedures. The formal mechanism used to combine the new information with the previously available information is known as the Bayes' theorem. Thus, the term Bayesian is applied to describe the statistical inversion approach, which is based on the following principles (Kaipio and Somersalo, 2004):

1. All variables included in the model are modeled as random variables;
2. The degree of information concerning these variables is coded in probability distributions;
3. The solution of the inverse problem is the posterior probability distribution.

The vectors containing the sought parameters, $\mathbf{P}$, and the experimental measurements, $\mathbf{Y}$, appearing in Eq. (44), are givem by, respectively:

$$\mathbf{P} \equiv [P_1, P_2, ..., P_{N_p}]^T, \qquad \mathbf{Y} \equiv [Y_1, Y_2, ..., Y_{N_m}]^T \tag{42, 43}$$

where N_p is the number of unknown parameters and N_m is the number of measurements. Bayes' theorem is stated as follows:

$$\pi_{posterior}(\mathbf{P}) = \pi(\mathbf{P}|\mathbf{Y}) = \frac{\pi_{prior}(\mathbf{P})\pi(\mathbf{Y}|\mathbf{P})}{\pi(\mathbf{Y})} \tag{44}$$

with $\pi_{posterior}(\mathbf{P})$ being the posterior probability density, $\pi_{prior}(\mathbf{P})$ is the prior density, $\pi(\mathbf{Y}|\mathbf{P})$ is the likelihood function and $\pi(\mathbf{Y})$ is the marginal probability density of the measurements, which plays the role of a normalizing constant.

In this work, it assumed the that the errors in the measured temperatures are additive, uncorrelated and normally distributed with zero mean and known covariance matrix $\mathbf{W}$. Than, the likelihood function can be defined as (Abreu et al., 2018):

$$\pi(\mathbf{Y}|\mathbf{P}) = (2\pi)^{-N_m/2}\,|\mathbf{W}|^{-1/2}\,\exp\Big\{-\frac{1}{2}[\mathbf{Y}-\mathbf{T}(\mathbf{P})]^T\mathbf{W}^{-1}[\mathbf{Y}-\mathbf{T}(\mathbf{P})]\Big\} \tag{45}$$

where $\mathbf{T}(\mathbf{P})$ is the vector of calculated temperatures, obtained from the solution of the forward problem with an estimate for the parameters $\mathbf{P}$.

In order to obtain an approximation of the posterior distribution for the unknown parameters, the Monte Carlo Method with Markov Chains (MCMC) will be used within the inverse analysis, according to the Metropolis-Hastings algorithm, considering the transition density as a uniform distribution. The steps of this algorithm are (Orlande and Fudym, 2017):

1. The chain starts with the initial state $\mathbf{P}^0$;
2. Sample a candidate $\mathbf{P}^*$ given the current state, $\mathbf{P}^{(i-1)}$, from a proposal distribution q($\mathbf{P}^*$, $\mathbf{P}^{(i-1)}$);
3. Calculate the acceptance factor: $$\beta = min\left[1, \frac{\pi(\mathbf{P}^*|\mathbf{Y})q(\mathbf{P}^{(i-1)}, \mathbf{P}^*)}{\pi(\mathbf{P}^{(i-1)}|\mathbf{Y})q(\mathbf{P}^*, \mathbf{P}^{(i-1)})}\right] \tag{46}$$
4. Generate a random value U that is uniformly distributed on (0, 1);
5. If $U \leq \beta$, define $\mathbf{P}^{(i)} = \mathbf{P}^{(*)}$; otherwise, define $\mathbf{P}^{(i)} = \mathbf{P}^{(i-1)}$;
6. Do $i = i + 1$ and return to step (2).

In this way, a sequence is generated to represent the posterior distribution and inference on this distribution is obtained from inference on the sample $\{\mathbf{P}^{(1)}, \mathbf{P}^{(2)}, ..., \mathbf{P}^{(t)}\}$, where t is the chain size. It is important to note that values of $\mathbf{P}^{(i)}$ must be ignored while the chain has not converged to equilibrium (the burn-in period).

4. RESULTS AND DISCUSSIONS

The solution to the heat transfer problem in this work involves the analysis of abrupt transitions between tissues layers. The epidermis layer is disregarded due to its negligible thickness and relatively small thermal influence in this case. Due to the abrupt nature of the transitions, a smoothing function, $\Theta(x)$, is employed between the layers:

$$\Theta(x) = \sum_{n=1}^{Ns} \Theta_{n-1} + (\Theta_n - \Theta_{n-1})\delta_n(x), \qquad \delta_n(x) = \frac{1}{1 + e^{-\gamma_n \frac{(x-x_n)}{L}}} \tag{47, 48}$$

where Ns is the number of smoothing functions, $x_n \in [0,\, L]$ is the transition position between two adjacent layers of tissue and γ_n is a parameter for adjusting thermal properties. Table 1 presents the exact values of the parameters used in the solution of the heat transfer problem.

Table 1. Values of tissue and blood thermophysical properties. Extracted from Cotta et al. (2010).

Sample total thickness	$L = 0.042\,(\mathrm{m})$	Dermis properties	$\rho = 1200\,(\mathrm{kg/m^3})$
Metabolic heat generation	$q_m = 420\,(\mathrm{W/m^3})$		$c_p = 3300\,(\mathrm{J/kg\,^\circ C})$
Ambient temperature	$T_\infty = 20\,(^\circ\mathrm{C})$		$k = 0.45\,(\mathrm{W/m\,^\circ C})$
Effective heat transfer coefficient	$h = 10\,(\mathrm{W/m^2\,^\circ C})$		$l = 0.002\,(\mathrm{m})$
Adjustment parameter	$\gamma_n = 200$		$\omega = 0.00125\,(1/\mathrm{s})$
Subcutaneous tissue properties	$\rho = 1000\,(\mathrm{kg/m^3})$	Inner tissue properties	$\rho = 1000\,(\mathrm{kg/m^3})$
	$c_p = 2500\,(\mathrm{J/kg\,^\circ C})$		$c_p = 4000\,(\mathrm{J/kg\,^\circ C})$
	$k = 0.19\,(\mathrm{W/m\,^\circ C})$		$k = 0.5\,(\mathrm{W/m\,^\circ C})$
	$l = 0.01\,(\mathrm{m})$		$l = 0.03\,(\mathrm{m})$
	$\omega = 0.00125\,(1/\mathrm{s})$		$\omega = 0.00125\,(1/\mathrm{s})$
Arterial blood properties	$\rho_b = 1060\,(\mathrm{kg/m^3})$	Parameters in applied	$\gamma_t = 200$
	$c_b = 3770\,(\mathrm{J/kg\,^\circ C})$	heat flux function	$x_t = 10\,\mathrm{e}\,110\,(\mathrm{s})$
	$T_a = 37\,(^\circ\mathrm{C})$		$q = 1000\,(\mathrm{W/m^2})$

First, the approximate solution of the single domain approach to the eigenvalue problem with variable coefficients is examined. A convergence analysis is performed to determine the required number of terms in the temperature expansion. Table 2 illustrates the convergence behavior for the first five eigenvalues associated with the original problem, Eqs. (18) - (20). There is a convergence of five to six significant digits for $NT^* = 70$ when compared to $NT^* = 80$.

Table 2. Behavior of the convergence of the first five eigenvalues (μ_i) of the problem (18)-(20).

μ_i^2	$NT^* = 30$	$NT^* = 40$	$NT^* = 50$	$NT^* = 60$	$NT^* = 70$	$NT^* = 80$
1	0.000041418	0.000041398	0.000041392	0.000041388	0.000041388	0.000041387
2	0.000898910	0.000898670	0.000898570	0.000898530	0.000898520	0.000898510
3	0.002264800	0.002263500	0.002263000	0.002262800	0.002262700	0.002262700
4	0.005397400	0.005396800	0.005396600	0.005396500	0.005396500	0.005396500
5	0.009956700	0.009947100	0.009944400	0.009943200	0.009942700	0.009942700

Table 3 presents the convergence of the numerical solution of the temperature for the eigenvalue problem with variable coefficients, obtained by GITT, at different point of the tissue for time $t = 100\,\mathrm{s}$ as the truncation orders, NT, increases. Based on the quality of the convergence shown in Table 2, $NT^* = 70$ is fixed. For comparison purposes, the last column provides numerical results obtained with the Method of Lines implemented in the NDSolve routine of the *Wolfram Mathematica* platform with sufficient mesh refinement to achieve accurate results. It is possible to verify that, for the case where $NT = 10$, at least four significant digits are already fully converged to the temperature field over almost the entire domain when compared to the results obtained with $NT = 15$ to $NT = 30$ and the results acquired through NDSolve.

Table 3. Numerical convergence of temperature for the eigenvalue problem with variable coefficients for time $t = 100\,\mathrm{s}$ and $NT^* = 70$.

x	$NT = 5$	$NT = 10$	$NT = 15$	$NT = 20$	$NT = 25$	$NT = 30$	NDSolve
0	42.049	41.734	41.741	41.747	41.751	41.753	41.750
0.0042	36.630	36.793	36.785	36.791	36.793	36.791	36.790
0.0084	35.897	36.160	36.155	36.159	36.156	36.157	36.157
0.0126	36.871	36.620	36.621	36.622	36.621	36.621	36.621
0.0168	36.868	36.778	36.778	36.778	36.777	36.777	36.777
0.0252	36.810	36.948	36.948	36.948	36.948	36.948	36.948
0.0294	37.103	36.991	36.991	36.991	36.990	36.990	36.991
0.0336	37.185	37.016	37.016	37.016	37.016	37.017	37.017
0.0378	36.993	37.031	37.030	37.030	37.031	37.031	37.031
0.0420	36.856	37.035	37.036	37.034	37.035	37.035	37.035

For the inverse problem solution, initially, a sensitivity analysis of the parameters, P_j, is performed, in order to facilitate the comparison and the identification of non-correlated parameters. For that, we define the scaled sensitivity coefficients, S_{ij}, as:

$$S_{ij} \equiv P_j \frac{\partial T_i}{\partial P_j}, \qquad i = 1, 2, ..., n_m, \qquad j = 1, 2, ..., n_p \tag{49}$$

where n_m corresponds to the total number of measurements and n_p is the number of parameters to be estimated.

Figure 2 shows the temporal variation of the sensitivity coefficients for three parameters displayed in Eqs. (1)-(6) and a single sensor is used, located at the position $x = 0\,\mathrm{m}$.

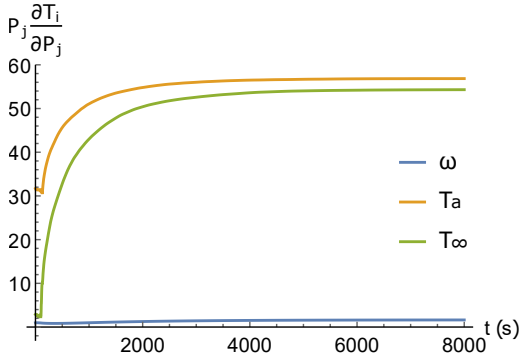

Figure 2. Sensitivity coefficients of the parameters

It can be noticed a low sensitivity in the perfusion term and a high sensitivity in the internal temperature and in the ambient temperature. Since the reference values for the internal temperature, T_a, and the ambient temperature, T_∞, can be found in the literature or measured, in this work is performed the blood perfusion rate estimation, ω, which is one of the essential parameters in applications such as clinical diagnostics employing infrared thermography (Bousselham, 2018).

For the RBF-based solution, it is used a set of 301 time measurements taken in the interval $0 \leq t \leq 600\,\mathrm{s}$ in the position $x = 0\,\mathrm{m}$. Table 4 shows the relative error, $|\epsilon_{rel}|$, between the solutions acquired by GITT and those obtained by RBF. It can be seen, for this case, that the average error decreases as the number of points used in the interpolation increases. It can also be observed a low value for the error, except for $\omega = 0.00100$ and $\omega = 0.00150$, which correspond to the boundaries of the sampled points employed in the RBF construction.

Table 4. Average percentage relative error between GITT and RBF results.

Points RBF	$\lvert\epsilon_{rel}\rvert\,(\%)$ $\omega = 0.00100$	$\lvert\epsilon_{rel}\rvert\,(\%)$ $\omega = 0.00110$	$\lvert\epsilon_{rel}\rvert\,(\%)$ $\omega = 0.00120$	$\lvert\epsilon_{rel}\rvert\,(\%)$ $\omega = 0.00130$	$\lvert\epsilon_{rel}\rvert\,(\%)$ $\omega = 0.00140$	$\lvert\epsilon_{rel}\rvert\,(\%)$ $\omega = 0.00150$
10	3.053600	0.289130	0.089532	0.083389	0.093620	17.03100
20	1.926200	0.292930	0.089363	0.083441	0.121310	14.86900
30	0.583960	0.290520	0.089308	0.082868	0.221820	2.828600

For the investigation of the solution of the inverse problem, we consider the vector of unknowns, $\mathbf{P} = \{\omega^*\}$, and a vector of synthetic experimental data, $\mathbf{Y}$, obtained by solving the direct problem calculated with the exact parameter and adding a noise given by a normal distribution, N, with zero mean and standard deviation, σ:

$$Y_i = T_i(\mathbf{P}_{exact}) + \varepsilon_i, \qquad \varepsilon \sim N(0,\, \sigma) \tag{50}$$

where $\mathbf{P}_{exact} = \{0.00125\}$ and $\sigma = 0.5\,^{\circ}\mathrm{C}$.

Table 5 presents six cases for the blood perfusion term estimation considering different numbers of points in the RBF function in the range [0.00100, 0.00150]. The purpose of this analysis is to verify the ideal number of points to obtain an adequate estimate for the perfusion term. It can be noticed that, with the exception of case 1, estimates were obtained close to the exact value using 10 or 30 points in RBF. When employing 20 points, the estimates in cases 1 and 6 (extremes of the interval) did not converge to values close to the exact one.

Table 5. Results of the simulations performed. Exact parameter value $\omega = 0.00125$.

		10 Points RBF	20 Points RBF	30 Points RBF
Case	Inicial state	Estimative ω^*	Estimative ω^*	Estimative ω^*
1	$\mathbf{P}^0 = \{0.00100\}$	0.0010070	0.0010062	0.0010034
2	$\mathbf{P}^0 = \{0.00110\}$	0.0012578	0.0012531	0.0012497
3	$\mathbf{P}^0 = \{0.00120\}$	0.0012584	0.0012480	0.0012493
4	$\mathbf{P}^0 = \{0.00130\}$	0.0012601	0.0012558	0.0012501
5	$\mathbf{P}^0 = \{0.00140\}$	0.0012528	0.0012518	0.0012594
6	$\mathbf{P}^0 = \{0.00150\}$	0.0012619	0.0014598	0.0012530

Table 6 shows six simulations to estimate the perfusion rate for different initial states. In all cases, 30 points, generated in the same range used in Table 5, are applied for interpolation with the RBF width value of $\eta = 2 \times 10^{-5}$. The results are obtained by the Monte Carlo Method with Markov Chains in the absence of prior information and using an uniform transition density. All cases present good accurate estimates, except for case 1, which did not converge to an approximate value of the perfusion term. It can also be observed a low cost computational. The simulations were performed on a computer with an Intel Core i7-7700k CPU @ 4.20 GHz with 16 GB of DDR4 RAM.

Table 6. Inverse problem results (exact value $\omega = 0.00125$).

Case	Inicial state	Estimative ω^*	Chain size	Burn-in period	Computational cost
1	$\mathbf{P}^0 = \{0.00105\}$	0.0012554	10000	1000	117.64 s
2	$\mathbf{P}^0 = \{0.00110\}$	0.0012578	10000	1000	121.72 s
3	$\mathbf{P}^0 = \{0.00115\}$	0.0012565	10000	1000	120.36 s
4	$\mathbf{P}^0 = \{0.00135\}$	0.0012508	10000	1000	119.45 s
5	$\mathbf{P}^0 = \{0.00140\}$	0.0012566	10000	1000	118.67 s
6	$\mathbf{P}^0 = \{0.00145\}$	0.0012598	10000	1000	110.86 s

Figure 3 presents the evolution of Markov Chains and in Figure 4 it is possible to observe the frequency histogram for initial estimate of $\mathbf{P}^0 = \{0.00145\}$, respectively. It is observed the convergence of the chains and that the histogram shows a Gaussian behavior.

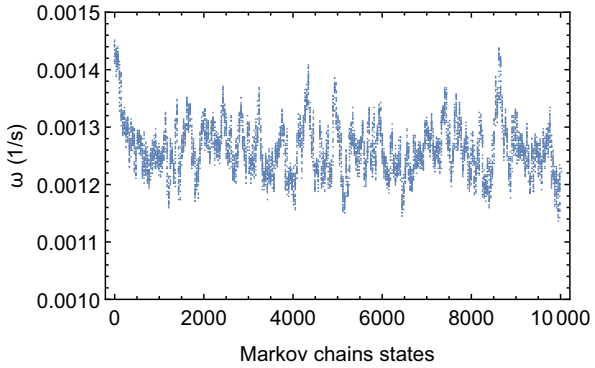

Figure 3. Markov chains - case 6

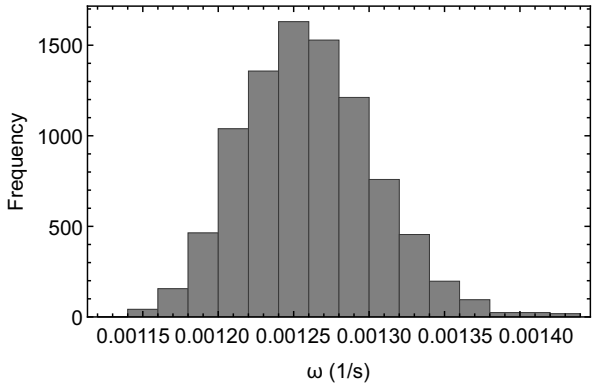

Figure 4. Frequency histogram - case 6

Figure 5 illustrates a comparison between the solution of the direct problem obtained by GITT and by metamodel with the exact value of $\omega = 0.00125$ and confirm the results presented in Table 4. Figure 6 illustrate the measurements data together with the solution obtained by the complete model using the estimated value $\omega^* = 0.0012598$. It is possible to observe, despite the noise employed in the experimental data, a good agreement between the curves.

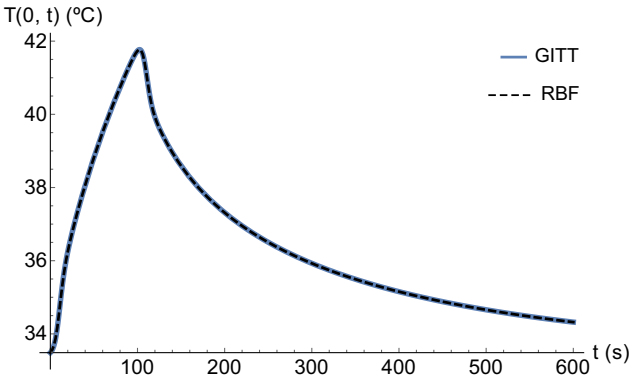

Figure 5. Transient behavior of the temperature field across the tissue thickness

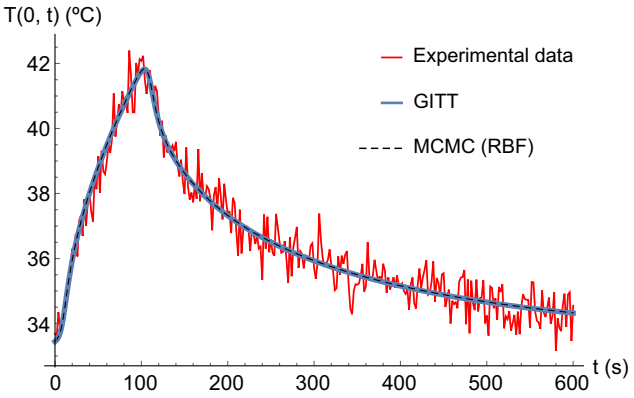

Figure 6. Simulated experimental measurements and temperature field obtained with ω^*

Figure 7 shows the behavior of the temperature profile over the total thickness of the tissues in $x \in [0, L]$ along the space variable for different times. It is noted that the surface region responds quickly to the external stimulus, and that this information is markedly decreased within the first two layers of the tissue structure, thus leaving the third layer unchanged. This behavior is clearly visible in Figure 8, for the 3-D plot of the temperature field along both the space and time variables. For plotting these graphs it was used $NT^* = 70$, $NT = 10$ terms and $\omega^* = 0.0012598$.

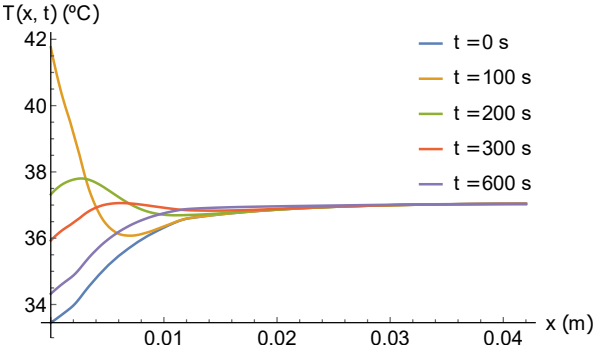

Figure 7. Behavior of the temperature field across the tissue thickness

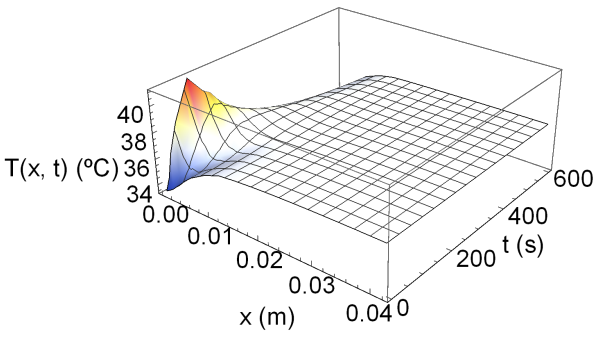

Figure 8. Profile of the estimated solution

5. CONCLUSION

The Generalized Integral Transform Technique was used to solve the heat transfer problem modeled by Pennes' equation. The results obtained for the direct problem reveal that the proposed approach results in accurate estimates of temperature distributions in heat transfer problems even for situations where there are abrupt variations in thermophysical properties.

An analysis of the inverse parameter estimation problem present in modeling a heat transfer problem in a biological system was performed. At first, a sensitivity analysis was performed, which demonstrated that the choices of the sensor location and the time interval in which the measurements will be acquired for use in solving the inverse problem must be carried out carefully, since they affect the reliability of the estimates.

A surrogate model based on Radial Base Functions is used to predict temperature distributions. The use of the metamodel in the prediction of temperatures proved to be an efficient tool both in the quality of the numerical results and in the low computational cost. Finally, the good results obtained demonstrate the feasibility of the approaches here proposed.

6. ACKNOWLEDGEMENTS

This study was financed in part by the Coordenação de Aperfeiçoamento de Pessoal de Nível Superior - Brasil (CAPES) - Finance Code 001. The authors also thank the funding agencies CNPq and FAPERJ.

7. REFERENCES

Abreu, L.A.S., Orlande, H.R.B., Colaço, M.J., Kaipio, J., Kolehmainen, V., Pacheco, C.C., Cotta, R.M., 2018. Detection of contact failures with the Markov chain Monte Carlo method by using integral transformed measurements, International Journal of Thermal Sciences 132, pp. 486–497.

Bousselham, A., Bouattane, O., Youssfi, M., Raihani, A., 2018. 3D brain tumor localization and parameter estimation using thermographic approach on GPU, Journal of Thermal Biology 71, pp. 52–61.

Cotta, R.M., 1993. Integral Transforms in Computational Heat and Fluid Flow, CRC Press, Boca Raton, Florida.

Cotta, R.M., Cotta, B.P., Naveira-Cotta, C.P., Cotta-Pereira, G., 2010. Hybrid integral transforms analysis of the bioheat equation with variable properties, International Journal of Thermal Sciences 49 (9), pp. 1510–1516.

Diller, K.R., Valvano, J.W., Pearce, J.A., 2000. Bioheat transfer. in: F. Kreith (Ed.), The CRC Handbook of Thermal Engineering. CRC Press, Boca Raton, FL, (Section 4.4).

Fornberg, B., Larsson, E., Wright, G., 2006. A new class of oscillatory radial basis functions. Computers and Mathematics with Applications, v. 51, pp. 1209–1222.

Haykin, S., 2008. Neural Networks and Learning Machines. 3. ed. New Jersey: Prentice Hall.

Jiang, S.C., Ma, N., Li, H.J., Zhang, X.X., 2002. Effects of thermal properties and geometrical dimensions on skin burn injuries, Burns 28, pp. 713–717.

Jin, R., Chen, W., Simpson, T.W., 2001. Comparative studies of metamodelling techniques under multiple modelling criteria, Struct Multidisciplinary Optim 23, pp. 1–13.

Kabiri, A., Talaee, M.R., 2019. Theoretical investigation of thermal wave model of microwave ablation applied in prostate Cancer therapy, Heat and Mass Transfer 55, pp. 2199–2208.

Kaipio, J., Somersalo, E., 2004. Statistical and Computational Inverse Problems, Applied Mathematical Sciences, vol. 160, Springer-Verlag, New York, USA.

Knupp, D.C., Naveira-Cotta, C.P., Cotta, R.M., 2012. Theoretical analysis of conjugated heat transfer with a single domain formulation and integral transforms, International Communications Heat and Mass Transfer 39 (3), pp. 355–362.

Orlande, H.R.B., Colaço, M.J., Dulikravich, G.S., 2008. Approximation of the likelihood function in the Bayesian technique for the solution of inverse problems, Inverse Problems in Science and Engineering 16 (6), pp. 677–692.

Orlande, H.R.B., Fudym, O., 2017. Thermophysical Properties Measurement and Identification, Handbook of Thermal Science and Engineering. 1 ed.: Springer International Publishing, pp. 01–40.

Pennes, H.H., 1948. Analysis of tissue and arterial blood temperatures in the resting human forearm, Journal of Applied Physiology 1, pp. 93–122.

Selmi, M., Dukhyil, A.A.B., Belmabrouk, H., 2019. Numerical Analysis of Human Cancer Therapy Using Microwave Ablation, Applied Sciences 10 (1).

8. RESPONSIBILITY NOTICE

The authors are solely responsible for the printed material included in this paper.